Dalton Transactions

Accepted Manuscript

ROYAL SOCIETY OF CHEMISTRY

www.rsc.org/dalton

Journal Name

RSCPublishing

ARTICLE

A facile approach to fabricate halloysite/metal nanocomposites with preformed and *in-situ* synthesized metal nanoparticles: A comparative study of their enhanced catalytic activity

Cite this: DOI: 10.1039/xoxxoooooox

Received ooth January 2012,
Accepted ooth January 2012

DOI: 10.1039/xoxxoooooox

www.rsc.org/

Sankar Das and Subhra Jana*

A widespread study has been carried out by the researcher during the last decades to improve the properties and performance of halloysite-based inorganic-organic hybrid nanocomposites (NCs) because of their excellent structural features and characteristics properties. Here, we report the fabrication of halloysite/metal nanocomposites in a large-scale through the immobilization of metal precursors followed by reduction or direct loading of preformed metal nanoparticles (NPs) over the surface of aminosilane modified halloysite nanotubes (HNTs), which in turn develops environmentally benign and low-cost heterogeneous catalysts. Characterization by different physical methods authenticates the successful fabrication of four different HNTs/metal NCs by these two different synthetic approaches, having monodispersed spherical morphology of the metal NPs. The catalytic activity and recyclability of all the NCs have been evaluated considering the reduction of 4-nitrophenol using sodium borohydride as a model reaction, attributing their almost comparable catalytic efficiency. However, a detailed kinetic study demonstrates the enhanced catalytic activity of *in-situ* synthesized HNTs/Ag among the four NCs, owing to the absence of any capping materials over the surface of NPs. Activation energy, pre-exponential factor, and entropy of activation have been estimated for this reduction reaction. A comparison study of their catalytic activity has been carried out with the reported heterogeneous catalysts, indicating the higher activity of these NCs for the reduction of nitroaromatics. Nevertheless, such an outstanding catalytic efficiency was only observed from HNTs/Au and HNTs/Ag NCs, with no activity from HNTs or aminosilane modified HNTs.

Introduction

The modern synthesis of the advanced functional materials with enhanced properties involves hybrid NCs, comprised of nanoscale inorganic materials and organic derivatives, where controlling the molecular structure at the atomic and macroscopic dimensions is a key aspect with a major effect on the performance. The quantum leap in hybrid NCs generally arises by reducing the domain size of the inorganic phase to several nanometers and generating huge interfacial areas, which introduces various covalent bonds or other compatibilization between the phases. Inorganic-organic hybrid NCs are astonishingly versatile and well known for their outstanding properties, such as high mechanical strength, thermal stability, high refractive index, low coefficient of thermal expansion etc.[1-4] These hybrid NCs can be synthesized from the diverse inorganic solids, like layered silicates clay, hydroxyapatite, silica, metal oxides, and a variety of biopolymers, e.g.;

polysaccharides, polypeptides, proteins, nucleic acids and so on.[5-8] The synthetic approach includes the structural templating of the inorganic component typically via self-assembly, preparation and surface modification of nanoscale inorganic particles, and use of nanometer-sized containers for synthesis.[9-11] They are of particular interest in advanced catalysis, controlled drug delivery, food processing, water purification, optics, electronics, mechanics, and sensors.[12-15]

Development of halloysite based inorganic-organic hybrid NCs opened up a new direction for the fabrication of novel materials and compound which will be explored as anti-corrosion agents, biocides, nanoreactor to host reactants for nanosynthesis and biomimetic synthesis. Halloysite nanotubes (HNTs) is a naturally occurring two-layered aluminosilicate clay ($Al_2Si_2O_5(OH)_4 \bullet nH_2O$) with a hollow tubular structure, formed by the surface weathering of aluminosilicate minerals, having constituent elements of aluminium, silicon, and oxygen. The adjacent alumina and silica layers with their water of hydration, result in a packing disorder and make the nanotubes to curve and roll up to form multilayers.[16,17] Formation of hallow tube is impelled by the mismatch in the periodicity between the oxygen sharing tetrahedral SiO_2 sheets and the adjacent octahedral AlO_6 sheets which also determine the inner positive and outer negative surface charges of the HNTs.[18,19] Thus, they possess different inner/outer surface chemistry which helps to manipulate the chemico-physical properties of these naturally available clay nanotubes through the control of the chemistry of the constituent elements as well as their morphology. Since hydrophilic surface of HNTs sometimes restricts their widespread applications in different filed, modification of the outer surfaces of these nanotubes with some organosilanes demonstrates improved dispersal of clay materials as well as enhances their physical, mechanical, and chemical properties. Furthermore, functionalization of HNTs by these organosilanes facilitates to immobilize metal nanoparticles (NPs) over the surface where HNTs behave as a solid support and organosilane acts as linker molecule and thus lead to the easy formation of HNTs/metal NCs.

Metallic nanoparticles have become the focus of basic research in modern nanoscience because of their unique properties which allows their efficient use in catalysis, photonics, electronics, and information storage.[20-23] Their properties and activity can be highly affected and reduced once they started agglomeration which tends to be bulk like materials. To prevent agglomeration and achieve well dispersed particles, we can either immobilized these NPs on solid supports or synthesize them directly over the supports.[12,24-28] However, a number of fundamental studies have been performed based on the supported noble metal NPs catalysts due to their high catalytic activity under mild condition, such as CO oxidation, hydrocarbon combustion, selective oxidation and hydrogenation, and water gas shift reaction.[28-34] Halloysite nanoclay, a cheap and an abundant natural resource, provides an alternative solid support for the immobilization of metal NPs to be utilized as a heterogeneous catalyst which subsequently gets separated from the reaction mixture at the end of the reaction and the use of HNTs as catalyst support is still very few.[17,35]

The primary objectives of our present study are to fabricate HNTs/metal NCs, probe the formation of the NCs, and then evaluate and compare their catalytic activity. HNTs/metal NCs were synthesized based on the immobilization of metal precursors over the surface of aminosilane modified HNTs followed by the reduction of the metal precursors to achieve NPs and the other approach involved direct immobilization of previously prepared metal NPs over HNTs surfaces. Exploiting these two approaches, HNTs/Au and HNTs/Ag NCs have successfully been synthesized and were authenticated by different physical methods. The spherical morphology of preformed Au and Ag NPs remained intact even after immobilization. The catalytic efficiency of all NCs has been demonstrated for the reduction of 4-nitrophenol by sodium borohydride and compared with the reported heterogeneous catalysts. We have estimated activation energy and entropy of activation for this reduction reaction. A detailed kinetic study represents that *in-situ* synthesized HNTs/Ag NCs are catalytically more active amongst the four NCs, although their catalytic efficiency is almost comparable and all these catalysts can be reused and recycled repetitively for this reduction reaction.

Experimental

Synthesis of aminosilane modified halloysite nanotubes

For surface modification of HNTs, a three-necked round bottom flask containing 2.0 g of HNTs and 20 mL of toluene, was fitted with a condenser, rubber septum, thermocouple adaptor, and quartz sheath in which a thermocouple was inserted. At 60 ^{O}C, 2.5 mL of (3-aminopropyl) triethoxysilane was injected to the flask which was heated with a heating mantle and the reaction solution was refluxed at 120 ^{O}C for 12 h. Afterwards the product was washed with toluene and ethanol respectively and dried at 100 °C under vacuum. The aminosilane modified HNTs were represented as HNTs-NH_2.

Fabrication of HNTs/metal nanocomposites with preformed metal nanoparticles

First, metal NPs were synthesized based on the thermal decomposition of a metal salt in a hot organoamine solvent.[36] All the reactions were carried out under a nitrogen atmosphere using standard air-free techniques. Gold(III) chloride trihydrate (0.12 mmol) was dissolved in a mixture of oleylamine (12 mM) and 1-octadecene (22 mM) in a flask which was fitted with a condenser, rubber septum, thermo-couple adaptor, and quartz sheath in which a thermocouple was inserted. The reaction flask was heated with a heating mantle to 120 ºC and aged for 30 min. Consequently, colour of the solution changed from yellow

to orange to pink indicating the formation of Au NPs. In a similar way, Ag NPs were synthesized from silver nitrate (0.12 mmol). Once the flask cooled down to room temperature, particles were collected by centrifugation after the addition of acetone-hexane (3:1) mixture and were redispersed in toluene and used as a stock solution for the immobilization over HNTs-NH_2. HNTs/metal nanocomposites were synthesized based on the immobilization of preformed metal NPs over the surface of silane modified HNTs. First, 0.5 g of HNTs-NH_2 was added to a beaker containing the previously synthesized Au NPs (6 mL) and stirred for 1 h to complete the immobilization of Au NPs onto the surface of HNTs-NH_2. A gradual fading of the intense pink colour of Au NPs solution to almost colourless while HNTs-NH_2 themselves turned pink, illustrated complete immobilization of Au NPs. Once the HNTs-NH_2 doesn't uptake additional Au NPs solution, the product was washed several times with toluene. Likewise, HNTs-NH_2 turned to yellow after the fabrication with Ag NPs, leaving behind a colourless supernatant solution. After the immobilization of Au and Ag NPs over HNTs-NH_2, the synthesized NCs are denoted as preformed HNTs/Au and HNTs/Ag respectively (please see Scheme 1).

Fabrication of HNTs/metal nanocomposites with *in-situ* synthesized metal nanoparticles

Alternatively, HNTs/metal nanocomposites were also synthesized based on the immobilization of metal precursors over the surface of HNTs-NH_2 followed by the reduction with ice cold aqueous solution of sodium borohydride. A beaker containing $HAuCl_4$ (6 mL, 10^{-2} M) and HNTs-NH_2 (0.5 g) was stirred on a magnetic stirrer for 6 h which in turn results a fading of the yellow colour of the solution, indicating immobilization of $HAuCl_4$ onto the surface of HNTs-NH_2. Once the HNTs-NH_2 get saturated with $HAuCl_4$, the product was washed several times with Mili-Q H_2O to remove the unadsorbed $HAuCl_4$ if any and reduced with ice cold aqueous solution of $NaBH_4$ to achieve *in-situ* HNTs/Au NCs. Similarly, HNTs/Ag NC was synthesized using $AgNO_3$ as a precursor, followed by the reduction with aqueous solution of $NaBH_4$ (see Scheme 1). The catalytic activity of these nanocomposites has been studied taking the reduction of 4-nitrophenol (4-NP) to 4-aminophenol (4-AP) as a model reaction.

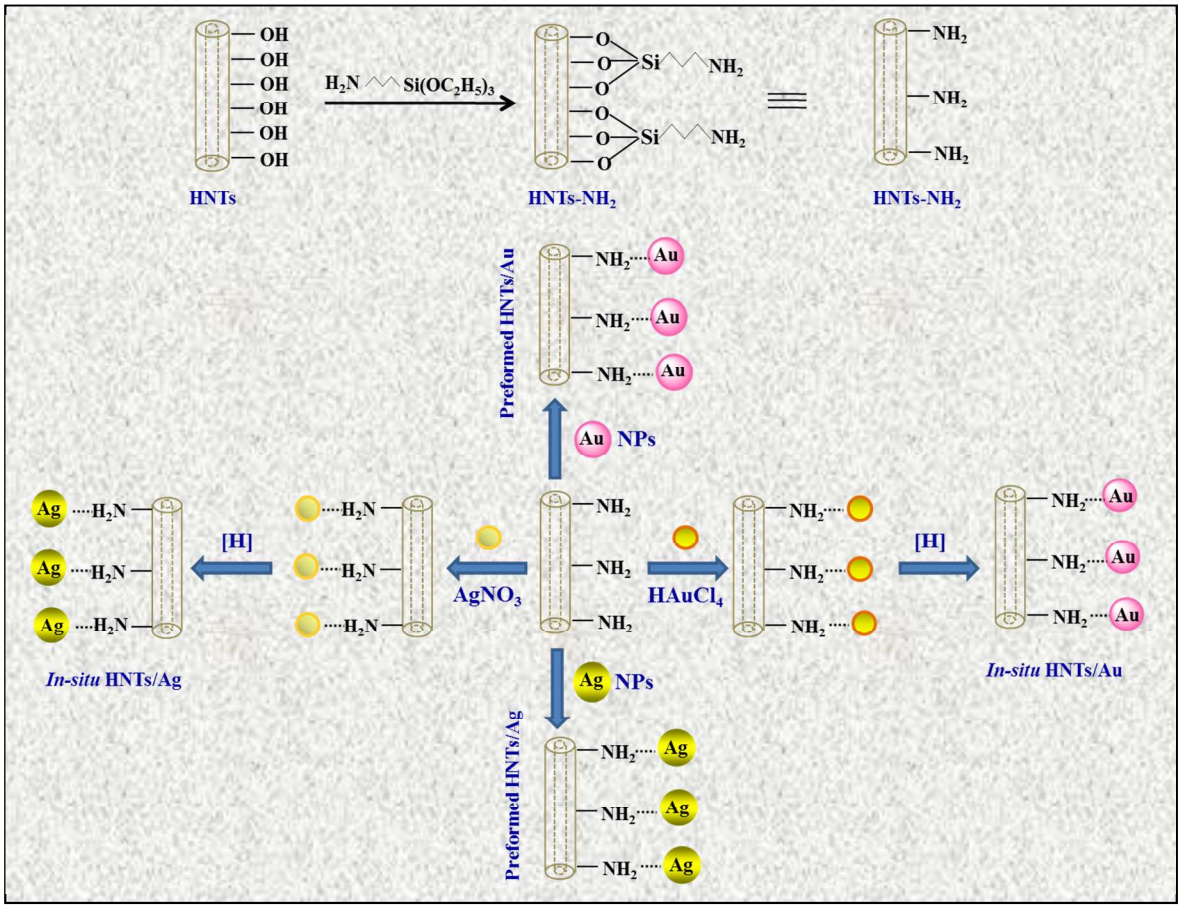

Scheme 1 Schematic presentation of the surface modification of halloysite nanotubes using (3-aminopropyl) triethoxysilane, subsequently fabrication of Au and Ag NPs decorated HNTs i.e.; HNTs/Au and HNTs/Ag nanocomposites which were achieved through the immobilization of (1) corresponding metal precursors followed by *in-situ* reduction and (2) previously synthesized metal NPs, over the surface of aminosilane modified HNTs.

Catalytic reaction

Catalytic activity of these four NCs has been studied for the reduction of 4-NP to 4-AP. In a standard quartz cuvette of 1 cm path length, 2.0 mg of HNTs/metal nanocomposites was taken along with 2.7 mL of aqueous solution of 4-NP (0.1 mM). Aqueous solution $NaBH_4$ (0.3 mL of 0.1M) was added to the reaction mixture and the time dependent absorption spectra were recorded at room temperature using a UV-Visible spectrophotometer.

Results and discussion

Characterization of nanocomposites

The different inner/outer surface chemistry of the clay nanotubes facilitates to manipulate the chemico-physical properties of HNTs through the control of the chemistry of their constituent elements. Hence, selective modification of the outer surface of HNTs (Scheme 1) has been performed through the grafting of an aminosilane which has been characterized by various physical methods. Fig. 1 represents the field emission scanning electron microscopy (FESEM) and transmission electron microscopy (TEM) images of HNTs before and after surface modification with (3-aminopropyl) triethoxysilane (APTES). HNTs composed of cylindrical shaped tubes with a typical length between 1.0 and 1.5 µm, having outer diameter of 50-100 nm and inner diameter of 15-20 nm. TEM image represents the cylindrical shaped tube composed of multilayer walls with an open-ended lumen, having defects on the outer surface of HNTs which are presumably due to the mechanical damage or by crystallographic defects. Compositional analysis by Energy dispersive X-ray analysis (EDX) indicates the presence of aminosilane after the surface modification of HNTs as they contain carbon and nitrogen along with the three main constituents of HNTs; oxygen, aluminium, and silicon (Fig. 1F). This is also confirmed by SEM-EDX elemental mapping which illustrates the presence of carbon and nitrogen in HNTs-NH_2. However, CHN elemental analysis demonstrates the immobilization of 0.39 mmol amino groups on one gram of HNTs-NH_2.

Fourier transform infrared (FTIR) spectroscopy ascertains the grafting of (APTES) over the surface of HNTs. FTIR spectra of HNTs and HNTs-NH_2 shown in Fig. S1A in Electronic Supplementary Information, indicate two characteristic bands at 3621 and 3697 cm^{-1} which can be attributed to the stretching vibrations of inner hydroxyl group and inner surface hydroxyl group respectively.[37] All these peaks further demonstrate the unaltered basic structure of HNTs even after surface modification though some new peaks are observed in HNTs-NH_2. Grafting of APTES over the surface of HNTs was confirmed due to the presence of new peaks at 2932 and 3453 cm^{-1} for the stretching vibration of C–H and N–H and at 1562 cm^{-1} for the N-H deformation. Fig. S1B represents the diffraction pattern of HNT-NH_2 which is similar to that of bare HNTs. The observed (020) reflection is the characteristic of tubular halloysite clay in both bare HNTs and HNTs-NH_2.[38] There is no intercalation of APTES into the interlayer of HNTs, as (001) reflection does not shift to the lower angles. This further assures that most of the hydroxyl groups are embedded and unavailable for grafting because of the multi-layer structure of HNTs.

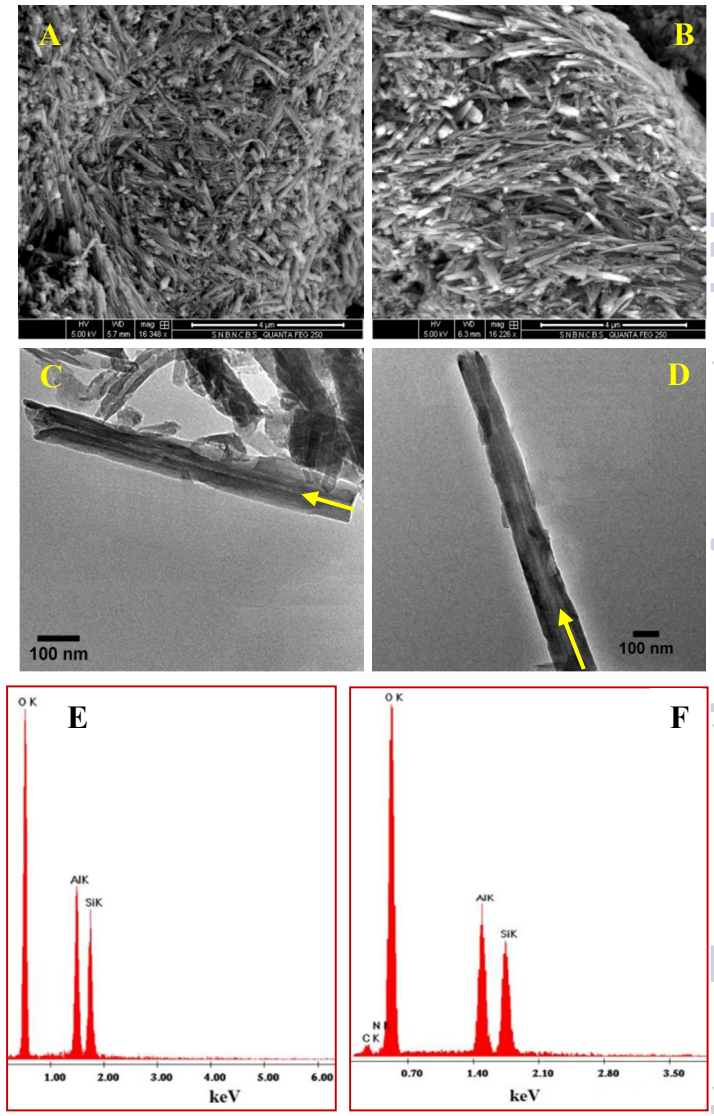

Fig. 1 FESEM and TEM images of HNTs (A & C) before and (B & D) after surface modification with an aminosilane, HNTs-NH_2. EDX spectra of (E) HNTs and (F) HNTs-NH_2.

The process of fabricating HNTs/metal NCs was elucidated in Scheme 1. After the surface modification of HNTs using APTES, HNTs/metal NCs were synthesized through the immobilization of both preformed and *in-situ* synthesized metal NPs over the surface of the clay nanotubes where the aminosilane behaves as a linker molecule and strengthen the interfacial adhesion of NPs over HNTs (see FTIR spectra in Fig. S2 in ESI). Based on the thermal decomposition of the metal salt in a hot organoamine solvent, we have synthesized Au and Ag NPs from their respective metal precursors (Fig. S3, ESI). A typical TEM image of Au NPs, shown in Fig. 2A, demonstrates nearly monodispersed spherical morphology with an average particle size of 9 ± 0.5 nm. Fig. 2B-D represents TEM images of HNTs/Au at different magnifications, indicating the immobilization of well-dispersed Au NPs over the surface of HNTs-NH_2 with no change in their size, shape, and morphology. TEM image of HNTs/Ag shown in Fig. 2E, also exhibits well-distribution of Ag NPs (8.5 ± 0.5 nm) over HNTs-NH_2 without any agglomeration. EDX spectra of HNTs/Au and HNTs/Ag demonstrate the obvious signals for Au and Ag respectively (Fig. S4, ESI). A comparison between the XRD patterns of HNTs and HNTs/Au or HNTs/Ag (Fig. 2F) establishes the presence of newly emerged peaks of (111) and (200) planes for face centered cubic (fcc) Au or Ag,[39] which further corroborate the loading of preformed Au and Ag NPs respectively, on the surface of amine modified HNTs.

In contrast to the fabrication of HNTs/metal NCs with preformed Au and Ag NPs, another synthetic strategy involved immobilization of their metal precursors over the surface of HNTs and then subsequent reduction to the corresponding metal NPs. In this approach, Au and Ag NPs were directly grown on the outer surface of HNTs-NH_2 to achieve HNTs/Au and HNTs/Ag NCs. After the addition and subsequent immobilization of $HAuCl_4$ or $AgNO_3$ on the surface of HNTs-NH_2, the adsorbed ions were reduced using aqueous solution of $NaBH_4$ which results in the formation of HNTs/Au and HNTs/Ag NCs respectively. The morphology and chemical composition of these *in-situ* synthesized NCs have also been characterized with the help of TEM and EDX analysis (Fig. 3). All the NPs are entirely immobilized and well dispersed over the surface of HNTs having particle sizes 9.0 ± 1.5 for Au and 9.0 ± 1.0 for Ag NPs respectively. EDX analysis and corresponding elemental mapping again demonstrate the *in-situ* formation of HNTs/Au and HNTs/Ag NCs. XRD patterns again determine fcc structure of the loaded Au or Ag NPs (Fig. S5, ESI).

Therefore, our both the synthetic routes (preformed and *in-situ*) helps to synthesize almost monodispersed spherical Au and Ag NPs with precise control over particle growth and morphology and are well distributed on the HNTs-NH_2 surfaces (Fig. S6, ESI). In our preformed HNTs/metal NCs, all the embedded NPs retain their size, shape, and morphology even after the immobilization. Thus, we have developed two different synthetic approaches to fabricate HNTs/metal NCs through the immobilization of preformed NPs as well as direct *in-situ* reduction with subsequent growth of the metal NPs over the surface modified HNTs, which in turn produce the heterogeneous catalysts.

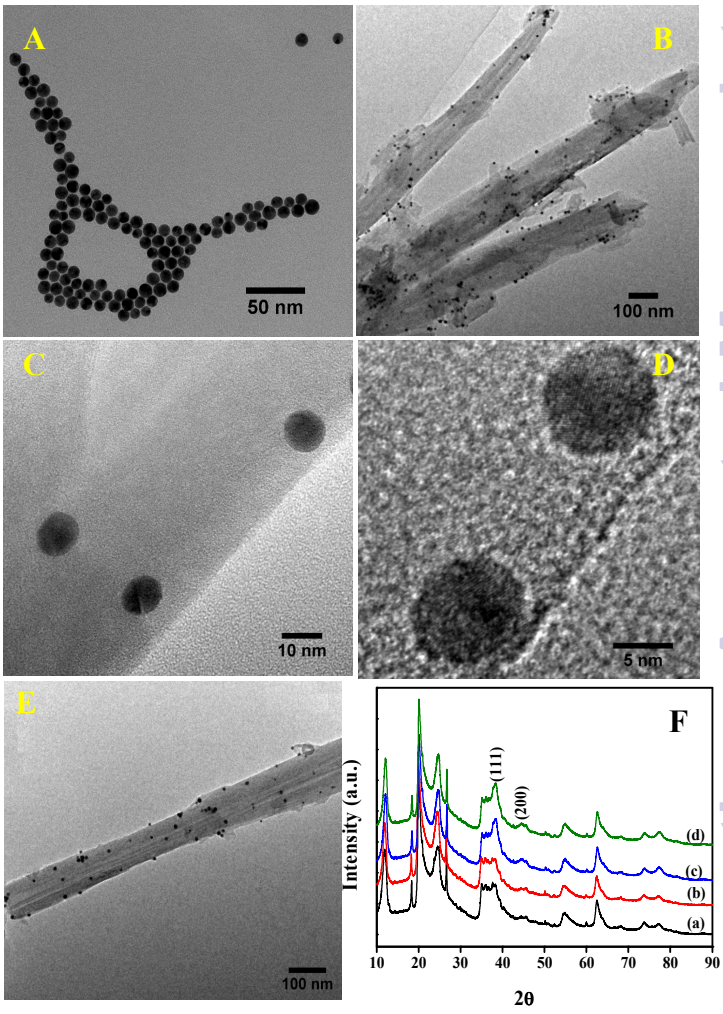

Fig. 2 (A) TEM images of (A) Au NPs before and (B-D) after immobilization on the surface of aminosilane modified HNTs (HNTs/Au NCs) at different magnifications. (E) TEM image of HNTs/Ag NCs prepared with preformed Ag NPs. (F) XRD patterns of (a) HNTs, (b) modified HNTs, HNTs/metal NCs synthesized with preformed (c) Ag and (d) Au NPs.

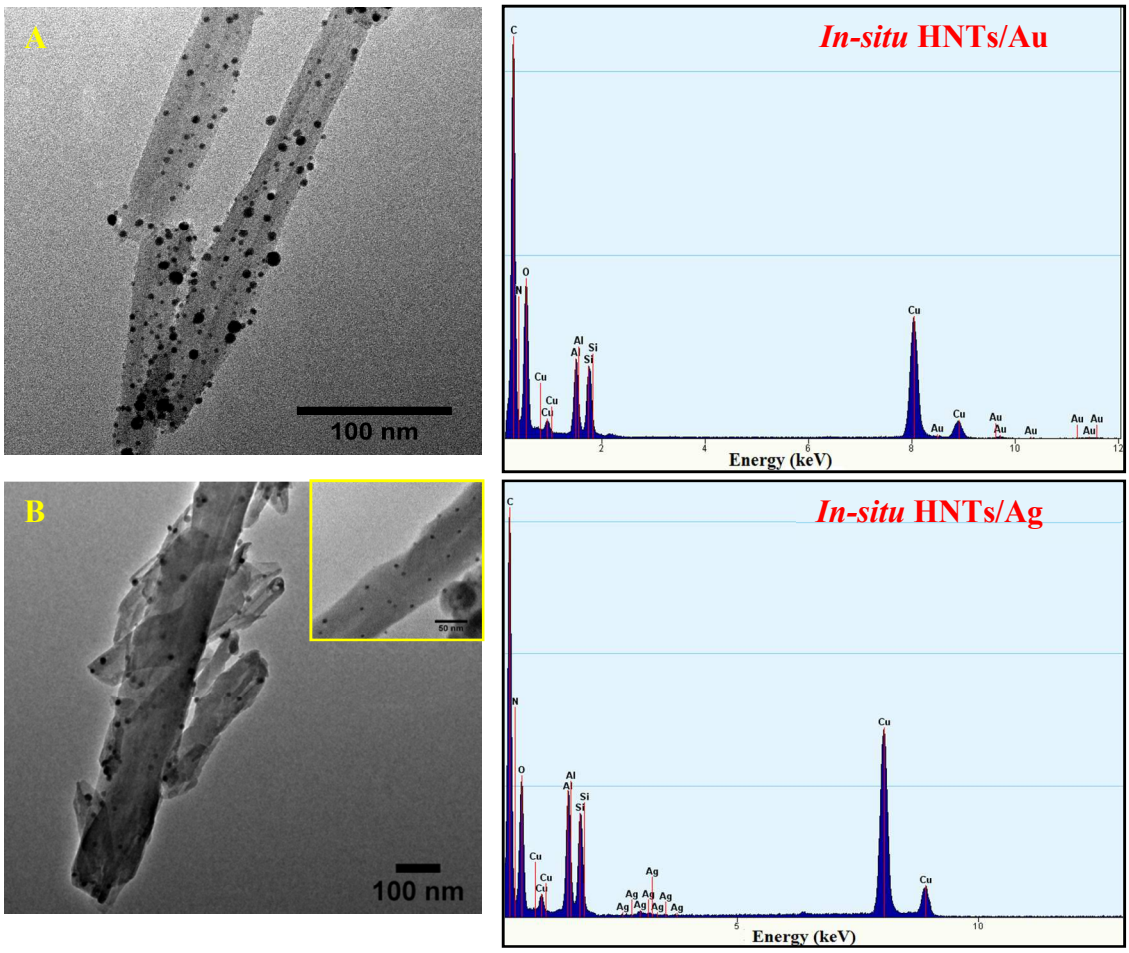

Fig. 3 TEM images of *in-situ* synthesized (A) HNTs/Au and (B) HNTs/Ag NCs and their corresponding EDX spectra, demonstrating the presence of Au and Ag NPs in HNTs/Au and HNTs/Ag NCs respectively.

Catalytic activity

Owing to the high surface-to-volume ratio, a potential application of metal nanoparticle is to catalyze certain reactions which would not be feasible otherwise. To evaluate and compare the catalytic activity of these NCs we have considered reduction of 4-nitrophenol (4-NP) by sodium borohydride ($NaBH_4$) as a model reaction. The reaction kinetics could be monitored using UV-Visible spectroscopy as color changes involved during the course of this reaction. An aqueous solution of 4-NP has a strong absorption (λ_{max}) at 317 nm under a neutral or acidic condition. After immediate addition of freshly prepared ice-cold aqueous solution of $NaBH_4$, the absorption peak was red shifted to 400 nm owing to the formation of 4-nitrophenolate ions as the alkalinity of the solution increased. In absence of any catalyst, though the reduction of 4-NP by $NaBH_4$ (E^0 for 4-NP/4-AP = -0.76 V and H_3BO_3/BH_4^- = -1.33V vs. NHE) is thermodynamically feasible but kinetically restricted. Thus, absorption intensity at 400 nm remained unaltered even for a couple of days without any catalyst. Addition of HNTs/metal NCs in the reaction mixture, caused a fading and ultimate bleaching of the yellow color, as well as the intensity of the absorption peak at 400 nm gradually decreased and a new absorption peak at ~300 nm appeared for 4-aminophenol (4-AP) which steadily increased in intensity as the reaction proceeded.[40,41] Time-dependent UV-Visible absorption spectra of 4-NP reduction reaction as a function of time in presence of *in-situ* synthesized HNTs/Ag NCs have been demonstrated in Fig. 4A. Two isosbestic points at 280 and 315 nm are observed in the UV-Visible spectra (in Fig. 4A), suggesting the precise conversion of 4-NP to 4-AP without any side reaction.[41,42] Sometimes the small bubbles of H_2 gas evolved from $NaBH_4$ during the reaction would retard the optical measurement and might lead to a shift of the UV-Visible spectra, resulting in the loss of the isosbestic points.

In the present study, the concentration of the reductant, borohydride ion largely exceeds to that of 4-NP. For all the experiments, concentration of 4-NP and $NaBH_4$ were maintaind to 0.1 and 10 mM respectively. Once we added $NaBH_4$ into the reaction solution, the metal particles embedded over HNTs

started the catalytic reduction by relaying electrons from the donor BH_4^- to the acceptor 4-NP only after the adsorption of both onto the particle surfaces. The evolved H_2 from BH_4^- purged out air and prevented the aerial oxidation of 4-AP. Furthermore, evolution of gas bubbles of H_2 surrounding the catalyst particles helped in stirring the solution which facilitated to disperse the catalyst particles in the reaction mixture for a smooth reaction to occur throughout the reduction process. As the initial concentration of $NaBH_4$ was very high, it remained constant throughout the reaction. Hence, we have used pseudo-first-order kinetics with respect to 4-NP to determine the average catalytic rate constant (k) of this reaction. The reaction conversion was estimated from the ratio of the concentration C_t/C_0, which was proportional to the relative intensity of the UV-Vis absorbance at 400 nm. Here, C_t and C_0 are the concentrations of 4-NP at reaction time t and the initial stage; A_t and A_0 are the corresponding absorbance at 400 nm

respectively. As shown in Fig. 4B, the linear correlation between ln (A_t/A_0) and reaction time (t) was confirmed through pseudo-first-order kinetics. Fig. 4C and 4D demonstrate the absorbance versus time plot for preformed and *in-situ* synthesized HNTs/Ag NCs and HNTs/Au NCs catalysts respectively. The catalytic rate constant k, which determines the reaction rate for 4-NP reduction, was obtained from the liner plot of ln (A_t/A_0) against reaction time (t) for all NCs catalysts. As shown in Table 1, the catalytic rate constant k for *in-situ* synthesized HNTs/Ag NCs (0.62 min^{-1}) is significantly higher among the four NCs catalysts, having the lowest value of k for preformed HNTs/Au NCs. It should be pointed out that we didn't observe any induction time for this reduction reaction upon the addition of any NCs catalysts at room temperature. At lower temperature, regardless of the NCs catalysts, there is an induction time i.e.; a certain period of time required to proceed the reduction reaction.

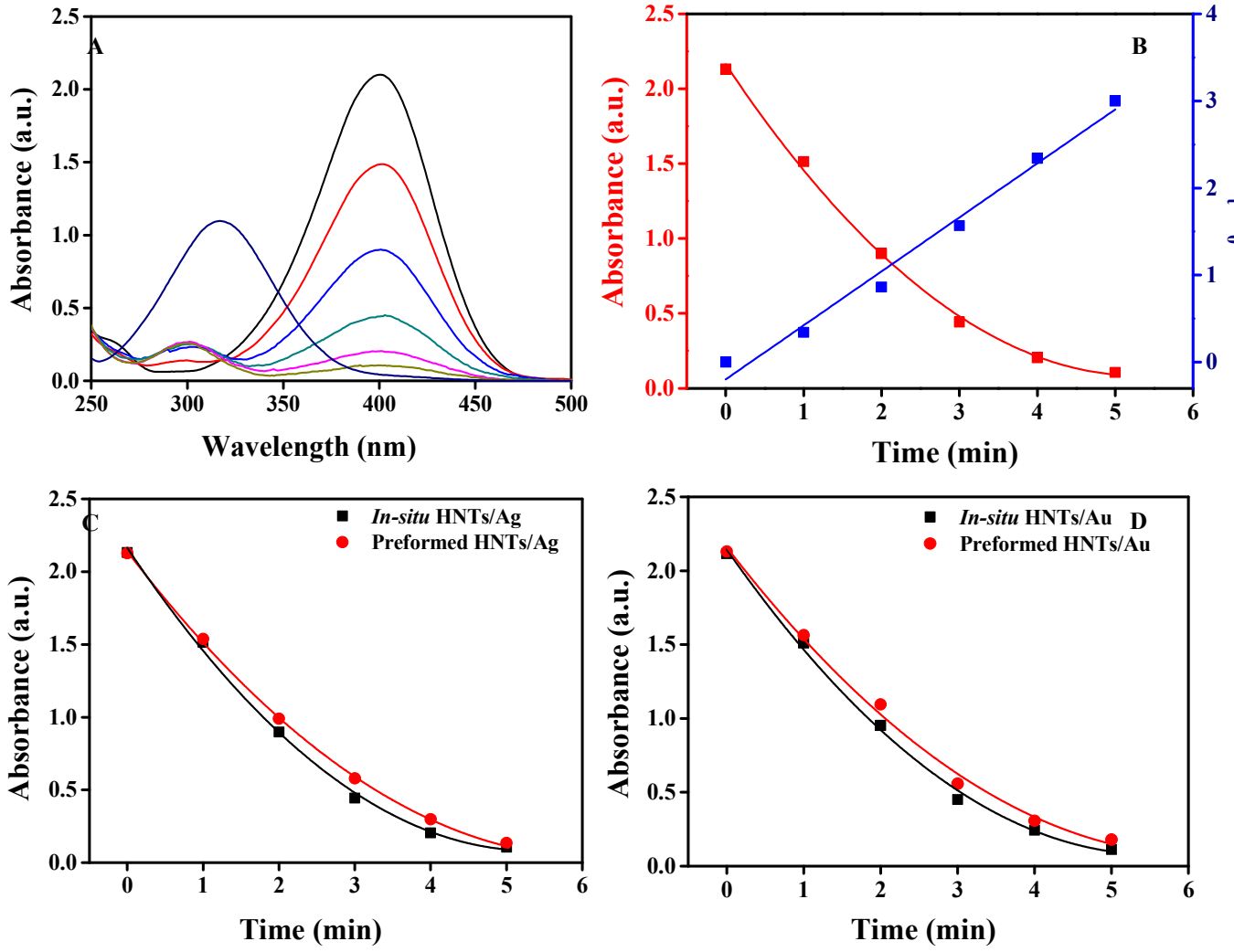

Fig. 4 (A) UV–Visible spectra for the successive reduction of 0.1 mM 4-NP using 0.1 M $NaBH_4$, catalyzed by 2.0 mg of *in-situ* synthesized HNTs/Ag NCs at an interval of 1 min and corresponding plot of (B) absorbance and ln A_t/A_0 against the reaction time for pseudo-first-order reduction kinetics of 4-NP. Plot of absorbance as a function of reaction time for 2.0 mg preformed and *in-situ* synthesized (C) HNTs/Ag and (D) HNTs/Au NCs respectively, to compare their catalytic activity.

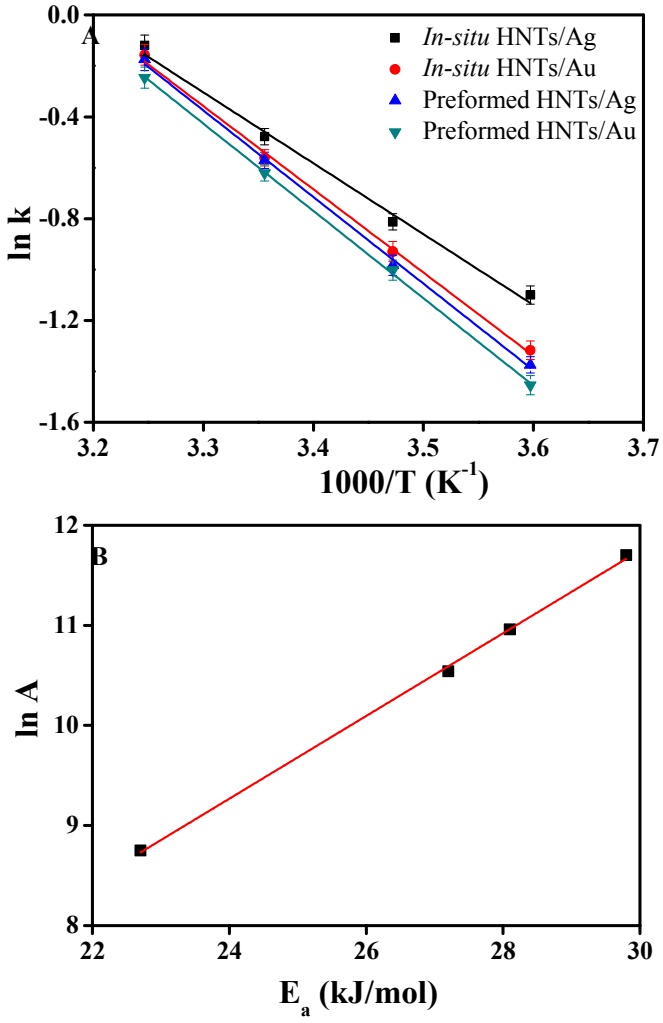

Fig. 5 (A) Arrhenius plots for the reduction reaction catalysed by preformed and *in-situ* synthesized HNTs/Ag and HNTs/Au NCs. Based on the linear correlation between ln k and the reciprocal of T, activation energy (E_a) has been calculated from the slope and pre-exponential factor from the intercept. (B) Plot ln A against E_a of the Arrhenius equation demonstrating the compensation effect for the NCs catalysts.

To estimate the apparent activation energy of this reaction, we have carried out the reaction at four different temperatures and evaluated the corresponding k which increases with increase in temperature, signifying the dependency of this reduction reaction on temperature. Based on the linear correlation between ln k and the reciprocal of T and following the Arrhenius equation: $ln\ k = ln\ A - E_a/RT$, we have measured the apparent activation energy (E_a) from the slope and the pre-exponential factor (A) from the intercept. Fig. 5 represents the Arrhenius plot for all the catalysts as well as plot of pre-exponential factors against activation energy of this reaction. The activation energy of the *in-situ* synthesized HNTs/Ag was estimated to be 23 kJ/mol, which is lower compared to preformed HNTs/Ag (28 kJ/mol) or HNTs/Au (30 kJ/mol) and even than that of *in-situ* synthesized HNTs/Au NCs (27 kJ/mol). The calculated values of activation energy reported in the literature vary considerably for different catalysts. Zeng et al. measured E_a for Au partially hollow nanoboxes (55 kJ/mol), hollow nanoboxes (44 kJ/mol) and nanocages (28 kJ/mol).[43] Pal and co-workers reported E_a of 21 kJ/mol for Au/calcium-alginate and 31 kJ/mol for Au NPs loaded on resin beads and their dependency on particle size.[44,45] Activation energy has also been found to be 14 kJ/mol for colloidal Pt nanocubes and it became 12 kJ/mol after supported them on polystyrene microsphere.[46] Ballauff and co-workers demonstrated E_a of 40, 44 and 43 kJ/mol for Pt, Pd and Au NPs embedded in polyelectrolyte brushes respectively.[42,47] Activation energy has also been reported to be 38 kJ/mol for Au NPs deposited on commercially available poly(methyl methacrylate)[48] and 45 kJ/mol for Ag-deposited Fe_2O_3 NPs.[49] Based on the equation $\ln A = \Delta S/R$,[50] we have estimated the entropy of activation (ΔS) and presented in Table 1. It is worth noting that the lowest pre-exponential factor and the entropy of activation were observed for *in-situ* synthesized HNTs/Ag NCs, whereas preformed HNTs/Au NCs had the highest pre-exponential factor and the entropy of activation.

Table 1 Summary of the particle size, rate constant (k), activation energy (E_a), pre-exponential factor (A), and entropy of activation (ΔS) for four different nanocomposites.

Nanocomposites	Particle Size (nm)	First-Order Rate Constant (k, min^{-1})	E_a (kJ/mol)	A (min^{-1})	ΔS (J/mol.K)
In-situ HNTs/Ag	9.0 ± 1	0.62033	22.7	6.3×10^3	72.75
In-situ HNTs/Au	9.0 ± 1.5	0.57049	27.3	3.8×10^4	87.63
Preformed HNTs/Ag	8.5 ± 0.5	0.5649	28.1	5.8×10^4	91.12
Preformed HNTs/Au	9.0 ± 0.5	0.53765	29.8	1.2×10^5	97.27

Thus, the present study demonstrates that E_a indicates the temperature dependence of the catalytic rate constant k and enhanced catalytic activity of *in-situ* synthesized HNTs/Ag among the four NCs. The linear correlation between ln A and E_a perceived in this catalytic system, clearly attributes to the compensation effect which is generally found in both heterogeneous and a large number of homogeneous catalytic systems[43,51] and could be precisely explained with the help of switching theory. Based on the switching theory,[52] this effect may be associated with the switching in kinetics from a regime where the overall rate is dominated by the rate of activation of the reactant to a regime where the stability of the reaction product adsorbed on the surface of the catalyst becomes more important.

In any catalysis, feasible recovery of catalysts is a crucial step to make the process cost-effective and eco-friendly. At the end of the catalytic reduction, all the NCs catalysts remain active and recycled for this reduction reaction after separated them from the product through a simple filtration and with proper washing using distilled water and drying at room temperature. However, even after repetitive use no leaching of metal NPs into the reaction solution was observed, ascribing the stability of the NCs catalysts. Fig. 6 exhibits plot of catalytic rate constant k for 4-NP reduction over a number of cycles using the same batch of NCs catalysts, attributing the stability and recyclability of the catalysts. The catalytic reduction of other isomers of nitrophenol, picric acid, and nitrobenzoic acid was also successful in presence of these NCs catalysts and even after repetitive use they retained their size, shape, and morphology.

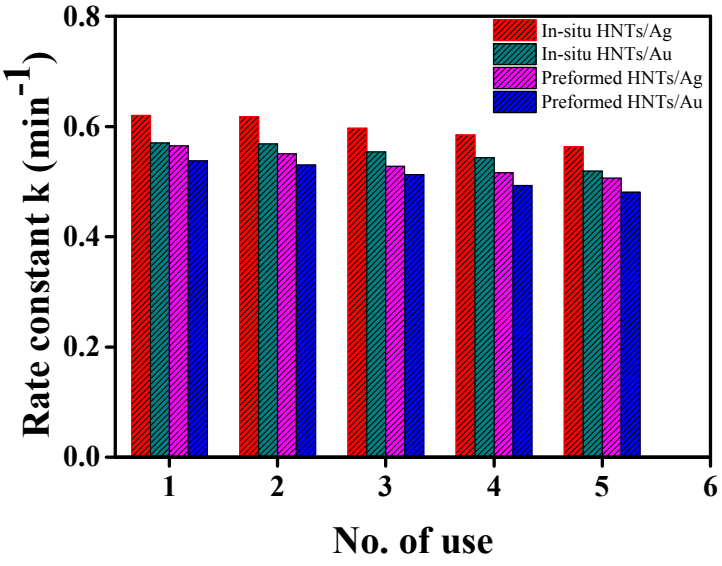

Fig. 6 Reusability of HNTs/Ag and HNTs/Au nanocomposites as catalysts for the reduction of 4-NP by $NaBH_4$, demonstrating the stability and recyclability of the nanocomposites.

Metallic nanoparticles strongly catalyze the redox reactions, which can be explained in terms of electrochemical current potential.[53,54] The mechanism of this reduction reaction using HNTs/metal NCs as catalyst can be explained based on the Langmuir−Hinshelwood model,[47,55] as shown in Fig. 7. Borohydride ions (BH_4^-) get adsorb onto the surface of metal and transfer a surface hydrogen species to the surface of the metal NPs. The adsorption of both BH_4^- and 4-NP molecules onto the surface of metal NPs are reversible and can be modeled by Langmuir isotherm. In this reaction, electron transfer takes place from BH_4^- to 4-NP only after the adsorption of both onto the surface of the metal NPs. The rate of electron transfer at the catalyst surface can be influenced by the adsorption of 4-nitrophenolate ion onto the catalyst surface and then interfacial electron transfer followed by desorption of the product, 4-aminophenol away from the surface, leaving a free metal surfaces which thus, accessible for a new catalytic cycle to proceed. It should be noted that the adsorption/desorption equilibriums and the diffusion of reactant molecules to the NPs are considered to be fast. The reaction between the adsorbed 4-NP and the metal NPs surface bound hydrogen atoms is the rate-determining step.

In order to compare the catalytic activity of our NCs catalysts with the catalysts reported in the literature, k was normalized to the concentration of Au or Ag, where k_{nor} ($k_{nor} = k/C_{metal}$) represents the intrinsic catalytic activity of the catalysts.[56] In Table 2, we have demonstrated the catalytic efficiency of our HNTs/metal NCs and compared with that of the reported catalysts, which comprised of Au and Ag NPs loaded on a support for the reduction of 4-NP. A remarkable catalytic activity for *in-situ* synthesized HNTs/Ag NCs was observed for this reduction reaction, having highest k_{nor} of 0.184 s^{-1} mM^{-1} in contrast to the other Ag catalysts, like Ag-NP/C composite (9.9×10^{-4} s^{-1} mM^{-1}),[57] Fe_3O_4@SiO_2-Ag magnetic nanocomposite (4.9×10^{-2} s^{-1} mM^{-1}),[58] Fe_3O_4@C@Ag composite microspheres (8.1×10^{-2} $s^{-1}mM^{-1}$),[59] AgNP-PG-5K (polyguanidino oxanorbornene, 0.149 s^{-1} mM^{-1})[60] etc. HNTs/Au NCs also have a reasonable catalytic activity for this reduction reaction and is higher than that of other heterogeneous Au catalysts e.g.; R-Au (Au NPs loaded on resin beads),[45] dendrimer-encapsulated gold nanoparticles,[61] Au-Chitosan/Fe_3O_4 (Au NPs on chitosan-coated iron oxide),[62] Au-Fe_3O_4 heterostructure,[63] and so on. *In-situ* synthesized HNTs/Au NCs shows a comparable catalytic activity, having k_{nor} of 0.17 s^{-1} mM^{-1}, to that of preformed HNTs/Au (0.16 s^{-1} mM^{-1}) and HNTs/Ag (0.168 s^{-1} mM^{-1}) NCs catalysts. Though the catalytic activity of preformed and *in-situ* synthesized HNTs/Au and HNTs/Ag NCs (i.e.; in presence and absence of stabilizing agent) are almost comparable, there is a still bit difference in their efficiency. The particle sizes of these four different NCs are almost similar, thus, the variation in their catalytic activity could be due to a difference in the available surface area of the metallic NPs during catalysis as well as a difference in the ability of the reactants to reach the NPs surfaces. In case of preformed HNTs/metal NCs, the presence

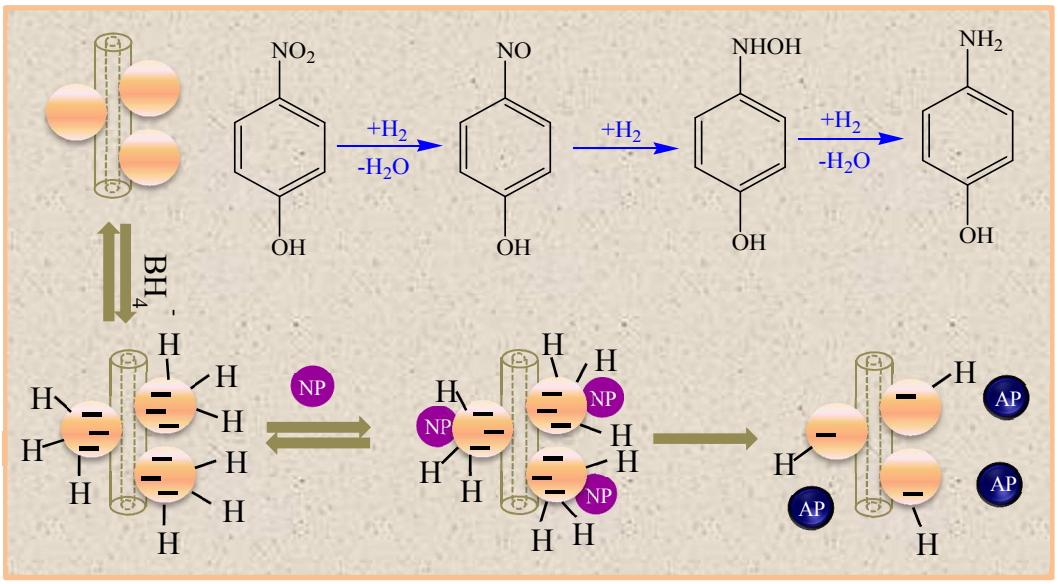

Fig. 7 Mechanistic model based on Langmuir–Hinshelwood mechanism for the reduction of 4-nitrophenol (4-NP) to 4-aminophenol (4-AP) using sodium borohydride ($NaBH_4$), catalyzed by metal nanoparticles (NPs) which were immobilized over the surface of aminosilane modified halloysite nanotubes (HNTs). Catalytic reaction takes place on the surface of metal NPs, once borohydride ions and 4-NP get adsorb onto the metal surface.

Table 2 Comparison of the catalytic rate constant (k) and normalized rate constants (k_{nor}) for different Ag and Au heterogeneous catalysts for the reduction of 4-nitrophenol (4-NP). C_{NP}: concentration of 4-NP, C_{Metal}: concentration of Ag or Au in the catalyst. Data were taken or calculated from the respective papers.

Catalysts	C_{NP} (mM)	C_{Metal} (mM)	K (s^{-1})	K_{nor} (s^{-1} mM^{-1})	Reference
Ag-NP/C composite	4.67×10^{-2}	1.7	1.69×10^{-3}	9.9×10^{-4}	57
Fe_3O_4@ SiO_2-Ag	6.1×10^{-2}	0.157	7.67×10^{-3}	4.9×10^{-2}	58
Fe_3O_4@C@Ag	5.0×10^{-2}	4.6×10^{-2}	3.72×10^{-3}	8.1×10^{-2}	59
AgNP-PG-5K	0.12	3.7×10^{-2}	5.5×10^{-3}	0.149	60
In-situ HNTs/Ag	0.1	5.6×10^{-2}	1.03×10^{-2}	0.184	Present work
Preformed HNTs/Ag	0.1	5.6×10^{-2}	9.42×10^{-3}	0.168	Present work
R-Au	0.1	1.4	5.85×10^{-5}	4.18×10^{-5}	45
Au/PAMAM	4.0×10^{-2}	0.95	2.0×10^{-3}	2.1×10^{-3}	61
Au-Chitosan/Fe_3O_4	0.1	0.17	1.2×10^{-2}	7.1×10^{-2}	62
Au-Fe_3O_4	4.33	0.88	1.05×10^{-2}	1.19×10^{-2}	63
In-situ HNTs/Au	0.1	5.6×10^{-2}	9.51×10^{-3}	0.17	Present work
Preformed HNTs/Au	0.1	5.6×10^{-2}	8.96×10^{-3}	0.16	Present work

of capping materials which are anchored over the surface of the NPs could make it sterically more difficult for the reactant molecules to reach the surface of the NPs and consequently they collide with each other. The considerable enhancement in the catalytic activity of *in-situ* synthesized HNTs/Ag NCs presumably ascribed to the higher affinity of Ag-N than that of Au-N, as well as the absence of any capping agent over the surface of NPs which results in the availability of the more exposed Ag atoms on the surface to get adsorb of the reactant molecules for a smooth reaction to occur. Hence, the efficacy of the NCs for the reduction of 4-NP follow the order: *in-situ* HNTs/Ag> *in-situ* HNTs/Au> preformed HNTs/Ag> preformed HNTs/Au. However, all HNTs/Au and HNTs/Ag NCs demonstrated such an outstanding catalytic efficiency, whereas bare HNTs or organosilane modified HNTs didn't exhibits any catalytic activity for this reduction reaction.

Conclusions

In the present study, based on the two different synthetic approaches, we have fabricated HNTs/metal NCs through the immobilization of preformed as well as direct *in-situ* growth of the metal NPs over the surface modified HNTs, which in turn develop efficient and low-cost heterogeneous catalysts. Thus, we have successfully prepared uniformly distributed Au and Ag NPs over the surface of HNTs in presence and absence of any coupling materials. Catalytic efficacy of these NCs has been studied for the reduction of nitroaromatics using $NaBH_4$ as a model reaction and the overall reaction mechanism was explained in terms of Langmuir-Hinshelwood model. Although their catalytic activity is almost comparable, a detailed kinetic study demonstrated the higher catalytic efficiency of *in-situ* synthesized HNTs/Ag NCs amongst the four NCs because of the absence of any capping agent over the surface of NPs. Activation energy, pre-exponential factor, and entropy of activation have been estimated for this reduction reaction. All these catalysts have been reused repetitively for this reduction reaction owing to their convenient recovery from the reaction solution through a simple filtration. This procedure demonstrates an added advantage for the efficient separation and recycling of the catalyst once the reaction completed, which is still a challenging task for homogeneous metal catalysts from both the economical and ecological point of view. Therefore, the process should be attractive because of its simplicity and large-scale production of the heterogeneous catalysts. The clay based nanocatalysts are relatively green catalysts, environmentally benign in nature, and a promising candidate for Au or Ag NPs based other catalytic applications in industrial syntheses.

Acknowledgements
The work was supported by the Department of Science and Technology (DST), New Delhi through DST INSPIRE faculty grant and JRF studentship from S. N. Bose National Centre for Basic Sciences, Kolkata, India.

Notes and references
Department of Chemical, Biological & Macro-Molecular Sciences
S. N. Bose National Centre for Basic Sciences
Sector-III, Block - JD, Salt Lake, Kolkata - 700 098, India
E-mail: subhra.jana@bose.res.in

† Electronic Supplementary Information (ESI) available: Materials, characterization techniques, FTIR spectra and XRD patterns of HNTs and HNTs-NH_2, UV-Visible absorption spectra of Au and Ag, EDX spectrum of preformed HNTs/Au nanocomposites, FTIR spectrum of HNTs/metal NCs, UV–Visible spectra for the 4-NP using preformed HNTs/Ag NCs. See DOI: 10.1039/b000000x/

1. C. Sanchez, B. Julián, P. Belleville and M. Popall, *J. Mater. Chem.*, 2005, **15**, 3559–3592.
2. G. L. Drisko and C. Sanchez, *Eur. J. Inorg. Chem.*, 2012, 5097–5105.
3. Z. Ahmad and J. E. Mark, *Mater. Sci. Eng. C*, 1998, **6**, 183–196.
4. K. H. Wu, T. C. Chang, Y. T. Wang and Y. S. Chiu, *J. Polym. Sci. A Polym. Chem.*, 1999, **37**, 2275–2284.
5. B. K. G. Theng, Formation and Properties of Clay–Polymer Complexes. *Elsevier, New York,* 1979.
6. X. Ding and S. M. Henrichs, *Mar. Chem.*, 2002, **77**, 225-237.
7. Y. Chen and J. O. Iroh, *Chem. Mater.*, 1999, **11**, 1218–1222.
8. C. C. Chang and W. C. Chen, *Chem. Mater.*, 2002, **14**, 4242–4248.
9. S. L. Burkett, S. D. Sims and S. Mann, *Chem. Commun.*, 1996, 1367-1368.
10. M. A. Ogawa, *Chem. Commun.*, 1996, 1149-1150.
11. D. G. Shchukin, G. B. Sukhorukov, R. R. Price and Y. M. Lvov, *Small*, 2005, **1**, 510-513.
12. S. Jana, S. Praharaj, S. Panigrahi, S. Basu, S. Pande, C. -H. Chang and T. Pal, *Org. Lett.*, 2007, **9**, 2191-2193.
13. A. F. Thunemann, D. Schutt, L. Kaufner, U. Pison and H. Mohwald, *Langmuir*, 2006, **22**, 2351-2357.
14. S. J. Tans, A. R. M. Verschueren and C. Dekker, *Nature*, 1998, **393**, 49-52.
15. S. Lelu, C. Novat, A. Guyot and E. Bourgeat-Lami, *Polym. Int.*, 2003, **52**, 542–547.
16. E. Joussein, S. Pitit, J. Churchman, B. Theng, D. Righi and B. Delvaux, *Clay Miner.*, 2005, **40**, 383-426.
17. Y. M. Lvov, D. G. Shchukin, H. Möhwald and R. R. Price, *ACS Nano*, 2008, **2**, 814-820.
18. E. Abdullayev, A. Joshi, W. Wei, Y. Zhao and Y. Lvov, *ACS Nano*, 2012, **6**, 7216- 7226.
19. G. Cavallaro, G. Lazzara and S. Milioto, *J. Phys. Chem. C*, 2012, **116**, 21932-21938.

20. D. B. Ingram, P. Christopher, J. L. Bauer and S. Linic, *ACS Catal.*, 2011, **1**, 1441–1447.
21. J. S. Lee, P. A. Ulmann, M. S. Han and C. A. Mirkin, *Nano Lett.*, 2008, **8**, 529-533.
22. L. R. Hirsch, R. J. Stafford, J. A. Bankson, S. R. Sershen, B. Rivera, R. E. Price, J. D. Hazle, N. J. Halas and J. L. West, *Proc. Natl. Acad. Sci.*, 2003, **100**, 13549-13554.
23. C. J. Murphy, A. M. Gole, S. E. Hunyadi and C. J. Orendorff, *Inorg. Chem.*, 2006, **45**, 7544-7554.
24. J. Dai and M. L. Bruening, *Nano Lett.*, 2002, **2**, 497-501.
25. S. Ivanova, V. Pitchon, Y. Zimmermann and C. Petit, *Appl. Catal. A*, 2006, **298**, 57-64.
26. S. Jana and S. Das, *RSC Adv.*, 2014, **4**, 34435-34442.
27. K. Esumi, R. Isono and T. Yoshimura, *Langmuir*, 2004, **20**, 237-243.
28. J. C. Garcia-Martinez, R. Lezutekong and R. M. Crooks, *J. Am. Chem. Soc.*, 2005, **127**, 5097-5103.
29. M. Haruta, S. Tsubota, T. Kobayashi, H. Kageyama, M. J. Genet and B. Delmon, *J. Catal.*, 1993, **144**, 175-192.
30. S. Jana, S. Pande, S. Panigrahi, S. Praharaj, S. Basu, A. Pal and T. Pal, *Langmuir*, 2006, **22**, 7091-7095.
31. J. A. Rodriguez, S. Ma, P. Liu, J. Hrbek, J. Evans and M. Pérez, *Science*, 2007, **318**, 1757−1760.
32. T. Fujitani, I. Nakamura, T. Akita, M. Okumura and M. Haruta, *Angew. Chem. Int. Ed.*, 2009, **48**, 9515−9518.
33. I. X. Green, W. Tang, M. Neurock and Jr. J. T. Yates, *Angew. Chem. Int. Ed.*, 2011, **50**, 10186−10189.
34. K. Shimizu, R. Sato and A. Satsuma, *Angew. Chem. Int. Ed.*, 2009, **48**, 3982−3986.
35. R. Wang, G. Jiang, Y. Ding, Y. Wang, X. Sun, X. Wang and W. Chen, *ACS Appl. Mater. Interfaces*, 2011, **3**, 4154–4158.
36. S. Jana, J. W. Chang and R. M. Rioux, *Nano Lett.*, 2013, **13**, 3618-3625.
37. P. Yuan, P. D. Southon, Z. Liu, M. E. R. Green, J. M. Hook, S. J. Antill and C. J. Kepert, *J. Phys. Chem. C*, 2008, **112**, 15742-15751.
38. W. O. Yah, H. Xu, H. Soejima, W. Ma, Y. Lvov and A. Takahara, *J. Am. Chem. Soc.*, 2012, **134**, 12134-12137.
39. S. Jana, S. Pande, A. K. Sinha, S. Sarkar, M. Pradhan, M. Basu, S. Saha and T. Pal, *J. Phys. Chem. C*, 2009, **113**, 1386-1392.
40. N. Pradhan, A. Pal and T. Pal, *Colloids Surf. A: Physicochem. Eng. Aspects*, 2002, **196**, 247-257.
41. S. Jana, S. K. Ghosh, S. Nath, S. Pande, S. Praharaj, S. Panigrahi, S. Basu, T. Endo and T. Pal, *Appl. Catal. A: General*, 2006, **313**, 41-48.
42. Y. Mei, Y. Lu, F. Polzer and M. Ballauff, *Chem. Mater.*, 2007, **19**, 1062–1069.
43. J. Zeng, Q. Zhang, J. Chen and Y. Xia, *Nano Lett.*, 2010, **10**, 30-35.
44. S. Saha, A. Pal, S. Kundu, S. Basu and T. Pal, *Langmuir*, 2010, **26**, 2885–2893.
45. S. Panigrahi, S. Basu, S. Praharaj, S. Pande, S. Jana, A. Pal, S. K. Ghosh and T. Pal, *J. Phys. Chem. C*, 2007, **111**, 4596-4605.
46. M. A. Mahmoud, B. Snyder and M. A. El-Sayed, *J. Phys. Chem. Lett.*, 2010, **1**, 28–31.
47. S. Wunder, F. Polzer, Y. Lu, Y. Mei and M. Ballauff, *J. Phys. Chem. C*, 2010, **114**, 8814–8820.
48. K. Kuroda, T. Ishida and M. Haruta, *J. Mol. Catal. A: Chem.*, 2009, **298**, 7–11.
49. K. S. Shin, J.-Y. Choi, C. S. Park, H. J. Jang and K. Kim, *Catal. Lett.*, 2009, **133**, 1–7.
50. R. Narayanan and M. A. El-Sayed, *Nano Lett.*, 2004, **4**, 1343.
51. J. J. Rooney, *J. Mol. Catal. A: Chem.*, 1998, **129**, 131.
52. T. Bligaard, K. Honkala, A. Logadottir, J. K. Norskov, S. Dahl and C. J. H. Jacobsen, *J. Phys. Chem. B*, 2003, **107**, 9325.
53. P. L. Freund and M. Spiro, *J. Phys. Chem. B*, 1985, **89**, 1074-1077.
54. D. S. Miller, A. J. Bard, G. Mclendon and J. Ferguson, *J. Am. Chem. Soc.*, 1981, **103**, 5336-5341.
55. M. A. Vannice, Reactions; Springer Science + Business Media: Philadelphia, PA, 2005.
56. Y. Fang and E. Wang, *Nanoscale*, 2013, **5**, 1843–1848.
57. S. Tang, S. Vongehr and X. Meng, *J. Phys. Chem. C*, 2010, **114**, 977-982.
58. Y. Chi, Q. Yuan, Y. Li, J. Tu, L. Zhao, N. Li and X. Li, *J. Colloid Interface Sci.*, 2012, **383**, 96−102.
59. Q. An, M. Yu, Y. Zhang, W. Ma, J. Guo and C. Wang, *J. Phys. Chem. C*, 2012, **116**, 22432-22440.
60. B. Baruah, G. J. Gabriel, M. J. Akbashev and M. E. Booher, *Langmuir*, 2013, **29**, 4225-4234.
61. H. Wu, Z. Liu, X. Wang, B. Zhao, J. Zhang and C. Li, *J. Colloid Interface Sci.*, 2006, **302**, 142-148.
62. Y. -C. Chang and D. -H. Chen, *J. Hazard. Mater.*, 2009, **165**, 664-669.
63. F. Lin and R. Doong, *J. Phys. Chem. C*, 2011, **115**, 6591–6598.

A facile approach to fabricate halloysite/metal nanocomposites with preformed and *in-situ* synthesized metal nanoparticles: A comparative study of their enhanced catalytic activity

Sankar Das and Subhra Jana*

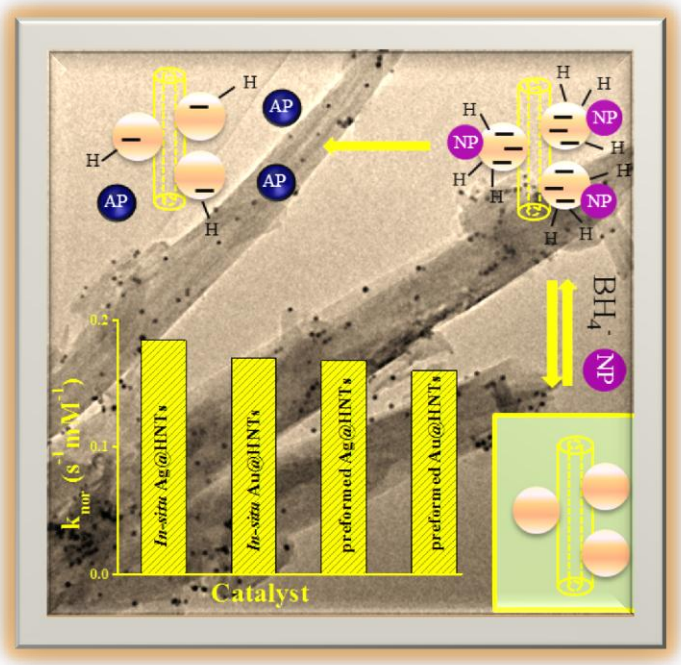

Halloysite/metal nanocomposites has been synthesized through the immobilization of preformed and in-situ synthesized metal nanoparticles over halloysite surfaces, which in turn produces efficient, cost-effective, and environmentally benign heterogeneous catalysts.